Continent and Life Evolution

OPEN ACCESS
Article

Mechanism of influence of root system distribution patterns on the shear strength of root-reinforced sand

Baoqin Lian, Chaoying Gu, Xingang Wang* and Haoyu Wang

***E-mail:** xgwang@nwu.edu.cn

Received 6 May 2026; Revised 10 July 2026; Accepted 13 July 2026; Published 4 August 2026

https://doi.org/10.55092/cle20260009

Graphical Abstract

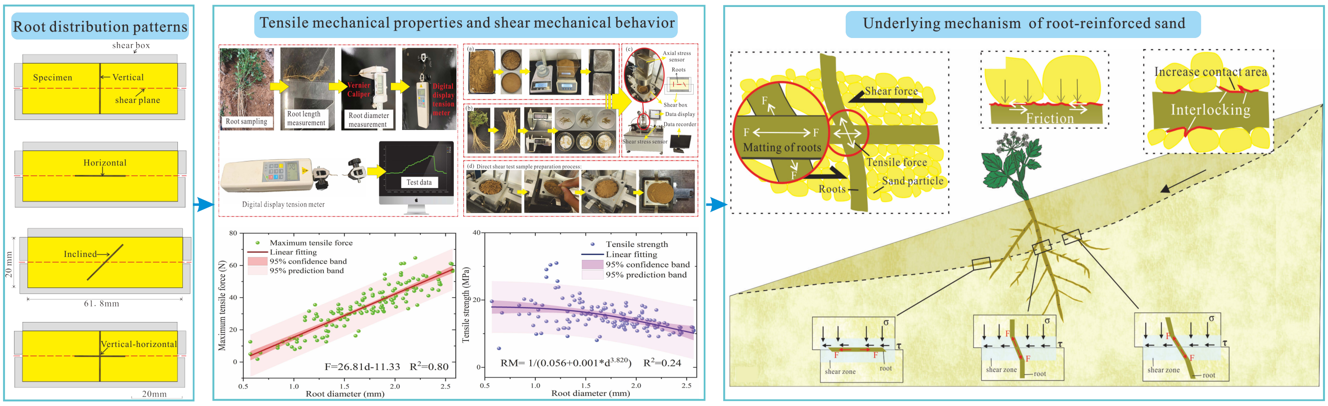

Highlights:

- Peak tensile force rises linearly with root diameter (F = 26.81d − 11.33, R^2 = 0.80).
- Root orientation, not quantity or diameter, dominates composite shear strength.
- Optimal setup: 1.5 mm roots, n = 6, inclined; cross networks peak cohesion (15.67 kPa).

Mechanism of influence of root system distribution patterns on the shear strength of root-reinforced sand

Baoqin Lian, Chaoying Gu, Xingang Wang* and Haoyu Wang

Digital Twin and Major Facility Disaster Prevention and Control Key Laboratory of Higher Education in Shaanxi Province, Northwest University, Xi'an 710069, China

***E-mail:** xgwang@nwu.edu.cn.

Abstract: Due to the loose and non-cohesive nature of sandy soil**,** road subgrade slopes in sandy regions are highly unstable, often experiencing adverse geological disasters such as shallow landslides and uneven settlement. To mitigate these hazards and promote sustainable development, vegetation root systems are frequently employed for slope stabilization. This paper investigates the reinforcing efficiency of roots in sand matrix via single-root tensile tests and mixed-level orthogonal direct shear tests. The tensile tests reveal that the peak tensile force (*F*) exhibits a robust linear increase with root diameter (d) ($F = 26.81d - 11.33$, $R^2 = 0.80$), whereas the ultimate tensile strength (*RM*) decays non-linearly via an inverse power function. Orthogonal direct shear tests demonstrate that root orientation is the governing factor controlling both composite shear strength and apparent cohesion, exhibiting a hierarchical influence priority of Orientation > Quantity > Diameter. Specifically, root inclusions primarily enhance the ultimate shear strength by increasing the cohesion, with negligible variation in the internal friction angle. The optimal root configuration for maximizing overall shear strength adopts 1.5 mm-diameter roots, a root number of 6, and an inclined orientation. Mechanistically, shear strength enhancement of the composite arises from a cooperative effect of interface friction, axial tensioning/anchoring, and structural interlocking, forming an anisotropic, parameter-specific system rather than a uniform strength upgrade. Thicker roots, under inclined or vertical arrangements, actively mobilize their tensile capacity (*F*) to resist shearing force. Conversely, three-dimensional vertical-horizontal (cross) networks maximize spatial confinement and structural interlocking, selectively optimizing the apparent cohesion to a peak value of 15.67 kPa. These findings provide a mechanical reference and root-architecture optimization strategies for slope stabilization projects in arid environments.

Keywords: root-reinforced soil; tensile test; shear strength; sandy soil; orthogonal test

1. Introduction

With expanding infrastructure development and intensifying impacts of climate change, desertification and slope instability have become critical challenges in the aeolian sand regions of northwest China (Wang *et al.* 2008; Qi *et al.* 2012). Due to its fine particle size and loose structure, aeolian sand subgrade slopes are highly susceptible to shallow landslides. To reduce the occurrence of these disasters and achieve sustainable development, ecological measures such as vegetation root reinforcement are increasingly favored over traditional engineering measures (Li *et al.* 2018; Lian *et al.* 2019) due to their lower costs, enhanced landscape effects (Sanchez-Castillo *et al.* 2019) and desertification control benefits (Gao *et al.* 2022).

The mechanical stabilization of slopes relies primarily on the capacity of plant roots to enhance soil shear strength (Operstein and Frydman 2000; Fan and Su 2008; Ghestem *et al.* 2014; Liu *et al.* 2026b). Previous studies using unconfined compressive strength tests, triaxial tests, and direct shear tests have shown that roots effectively transfer shear stresses from the soil matrix to the root network via tensile mobilization (Pollen 2007; Garg *et al.* 2015; Feng *et al.* 2020; Liu *et al.* 2026b). Additionally, transpiration by plant roots increases soil matric suction, a hydrological effect that also contributes positively to slope stability (Garg *et al.* 2015; Feng *et al.* 2020). Research by Natasha Pollen on the spatiotemporal variation of root reinforcement indicates that root pullout and breakage are related to soil shear strength and soil moisture (Pollen 2007). Most studies attribute the enhancement of soil shear strength by roots to the additional cohesion they provide (Schmidt *et al.* 2001; Kokutse *et al.* 2016; Feng *et al.* 2020).

Recent research has demonstrated that root architecture plays an important role in reinforcement efficiency (Ni *et al.* 2025). For instance, Wang *et al.*'s research on plant root forms suggested that R-type (most of the main roots grow obliquely) and V-type (plants with well-grown near-vertical roots) roots represent the most effective structures for hillside stability (Wang *et al.* 2020). Studies by Ng, Kamchoom, Leung *et al.* found that the heart-shaped root system provides greater hydrological and mechanical effects, leading to enhanced stability of shallow slopes (Ng *et al.* 2016). Although numerous studies have investigated the effects of root morphology on soil mechanics, most focus on the overall geometric morphology of plant roots, with few detailed studies of root diameter, quantity, and orientation. Furthermore, previous bio-geotechnical research has predominantly focused on loess or agricultural soils (Li *et al.* 2018; Lian *et al.* 2019; Liu *et al.* 2026a), while studies on the influence of roots on sandy soil are scarce. Therefore, to improve vegetation-based protection of shallow slopes in desert areas, investigating the shear strength and reinforcement mechanisms of root-soil composites in sandy soil is essential.

Accordingly, this study employs root tensile tests and direct shear tests to investigate the influence of root diameter, quantity, and distribution orientation on the shear strength parameters of sandy road slopes. The objectives are to identify the optimal reinforcement scheme and to elucidate the underlying reinforcement mechanisms. The study area is located in the Jizo Bend area of the Mu Us Desert, the largest desert in China. The surface soil is predominantly composed of aeolian sand, and slopes in this area are prone to frequent geohazards such as shallow landslides and surface erosion (Figure 1).

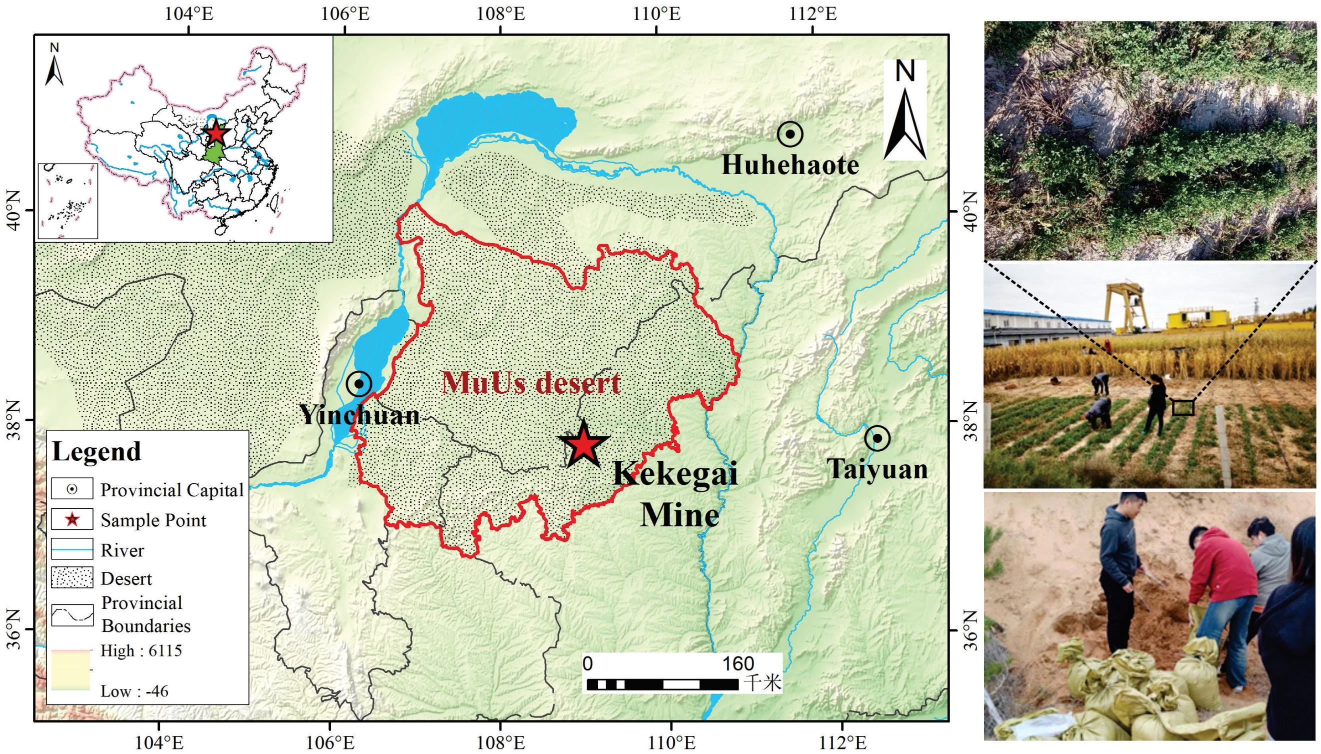

Figure 1. Map of the study area and sampling location.

2. Materials and methods

2.1. Test materials

2.1.1. Aeolian sand

The aeolian sand used in this study was collected from the Kekegai mining area in the Mu Us Desert. The regional surface soil consists predominantly of loose to medium-dense aeolian sand. Particle size analysis revealed that 98.36% of the sand grains fall within the 80–500 µm range. Following the Geotechnical Test Method Standard (China National Standards 2019), the basic physical and mechanical properties of the tested soil sample are presented in Table 1. Particle size distribution was determined using an MS-2000 laser particle size analyzer (MALVERN, UK), as shown in Figure 2. According to the geotechnical test standard (GB/T 50123) (China National Standards 2019), a well-graded sand must satisfy the criteria for the coefficient of uniformity ($C_u = \frac{d_{60}}{d_{10}}$) greater than 5 and the coefficient of curvature ($C_c = \frac{(d_{30})^2}{d_{10} \times d_{60}}$) between 1 and 3, where *d* refers to the effective diameter of the soil particles and subscripts (10, 30, and 60) denote the percentage of soil particles that are finer than that size. With C_u = 2.30 and C_c = 0.88, the sand in this region is classified as poorly graded and uniform. From a soil ecological perspective, this sand exhibits poor soil structure, low inorganic salt content, good permeability, and poor water and fertilizer retention capacity.

Table 1. Physical properties of undisturbed soil.

Dry density (ρ_d)	Water content (w)	Grain size fractions (%)			Coefficient of uniformity (C_u)	Coefficient of curvature (C_c)
		> 500 μm	250–500 μm	< 250 μm		
1.32 g/cm³	9.53%	1.64	41.29	57.07	2.30	0.88

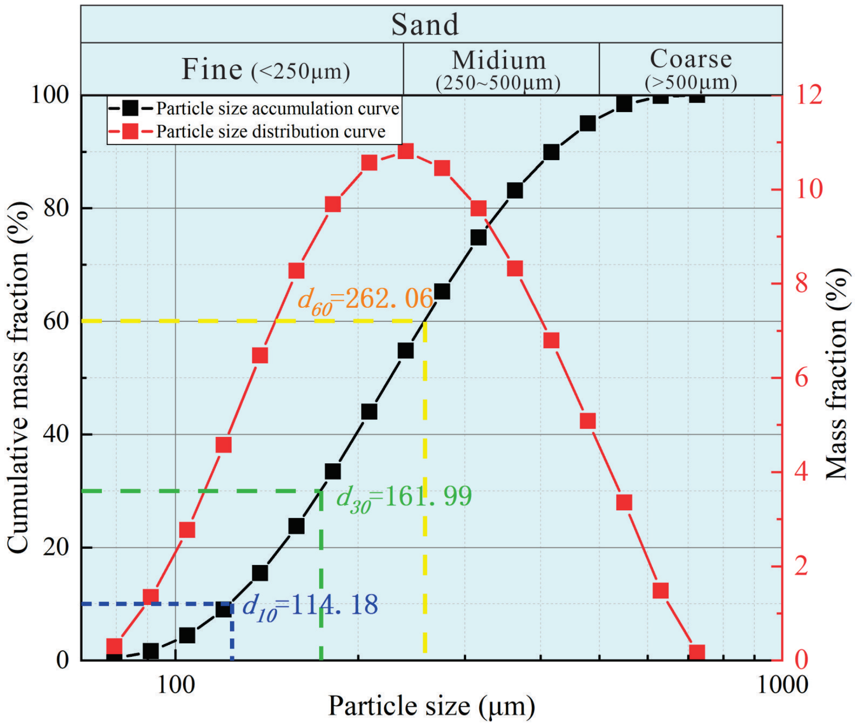

Figure 2. Grain size distribution curve of aeolian sand.

2.1.2. Plant roots

In a preliminary study, our research group utilized drilling mud from the Kekegai mining area to amend the local aeolian sand. Subsequent cultivation trials demonstrated that this mud amendment significantly enhanced the soil's suitability for vegetation growth. Given its drought tolerance, salt and cold resistance, high yield, excellent quality, and economic value, alfalfa is widely utilized as a staple leguminous forage species and a preferred choice for slope stabilization and ecological restoration (Duan *et al.* 2026). In this study, we selected alfalfa roots grown in the mud-amended aeolian sand from the planting trials. To account for potential biological differences arising from root location (Cazzuffi *et al.* 2014; Mao *et al.* 2018) and to control for variables, taproots located within 20 cm below the soil surface were selected from each plant for subsequent testing.

The test procedures were as follows: (1) After retrieving the plants, the above-ground stems and leaves were cut off. Most of the adhering soil was removed from the roots, which were then rinsed, blotted dry with absorbent paper, and air-dried for 24 hours. The cleaned roots were then stored at 4 °C to maintain freshness. (2) Roots with favorable growth characteristics were selected. Their diameters were measured, and they were classified accordingly; (3) Roots within each diameter class were cut into 5 cm lengths for tensile testing; (4) Selected roots were cut into 2 cm lengths for direct shear testing on root-reinforced soil with varying diameters, quantities, and distribution orientations. The root arrangements tested in the direct shear experiments are illustrated schematically in Figure 3. As shown, four distribution patterns were adopted: vertical (90°), horizontal (0°), inclined (45°), and vertical-horizontal (cross-intersecting). For the horizontal arrangement, the roots were placed parallel to the shear plane. In the vertical configuration, the roots span the entire height of the specimen, centered across the horizontal shear plane. For the inclined and cross-intersecting patterns, the segments are positioned symmetrically relative to the shear plane to ensure uniform mobilization of strength capacity during shearing.

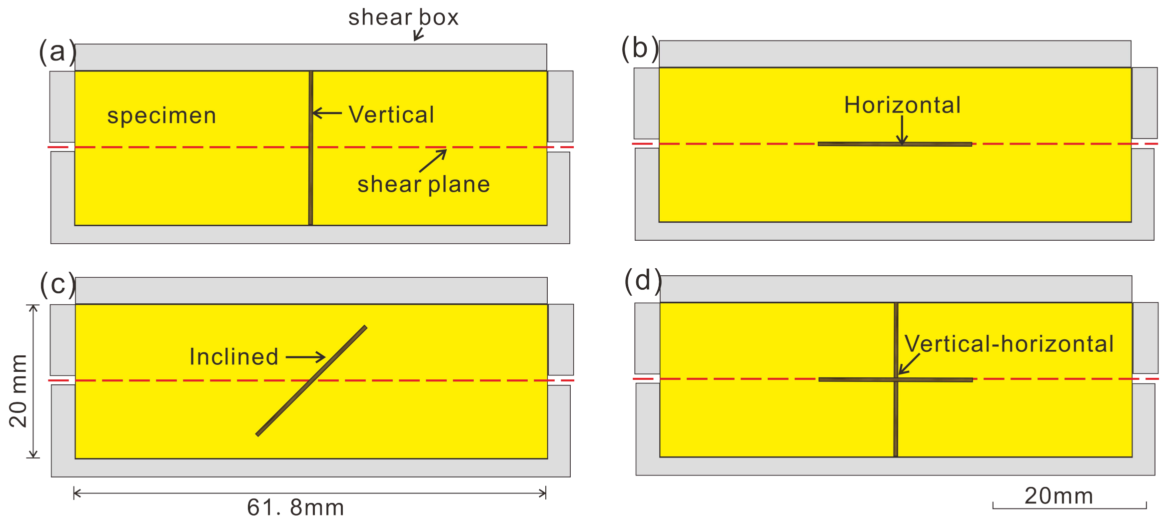

Figure 3. Schematic diagram of the four root distribution patterns within the 61.8 mm × 20 mm (diameter × height) direct shear box: **(a)** Vertical (90°); **(b)** Horizontal (0°); **(c)** Inclined (45°); **(d)** Vertical-horizontal (cross-intersecting).

2.2. Test methods

2.2.1. Tensile test

An Edburg HP-500 high-precision digital push-pull tension meter (range: 0–500 N, accuracy: ±0.1 N) was used to directly record and store tension data during the pulling process. The test employed two fixtures: the first was connected to the tension meter to transmit the tension value during pulling, while the second, whose opposite end was fixed (Figure 4), gripped the other end of the root. The specific test procedure was: (1) Roots were cut to 5 cm in length. For each root, diameters were measured at the top, center, and bottom positions (1 cm from each end and the midpoint) using vernier calipers, and the average of these readings was taken as the root's mean diameter. (2) To avoid initial tautness or curvature, both ends of the root were wrapped in medical cotton cloth before being clamped by the fixtures. (3) The tension meter's data recording system was turned on. Upon root failure, the rupture location was observed. Tests with ruptures occurring near the fixtures—potentially affected by clamping effects—were discarded as invalid. Conversely, tests with ruptures in the middle section of the root were accepted, from which both data and the force-displacement curve were recorded.

The relationship between the tensile strength of alfalfa roots and root diameter was determined through the experiment. Tensile strength was calculated according to Equation (1). Ultimately, approximately 136 alfalfa roots with relatively complete growth and diameters ranging from 0.5 mm to 3.0 mm were selected for the tests.

The relationship between tensile strength and maximum tensile force is:

$$RM = \frac{4F}{\pi d^2} \quad (1)$$

Where *RM* is the root tensile strength (MPa), *F* is the maximum tensile strength (N), and *d* is the root diameter (mm).

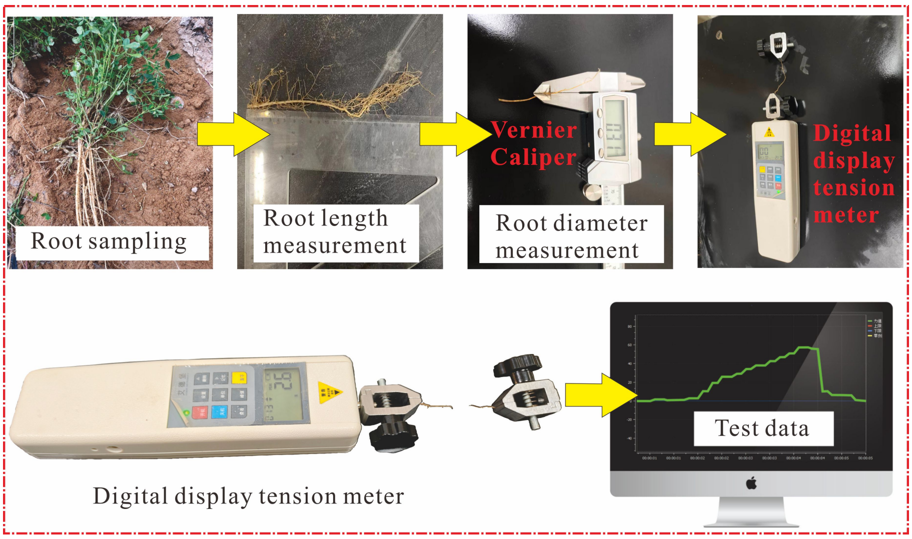

Figure 4. Flowchart of the tensile test.

2.2.2. Direct shear test

The direct shear test was performed using a TT-ADS automatic single-coupled direct shear instrument (Figure 5c), with a sample size of 61.8 mm in diameter × 20 mm in height (using a ring cutter). Before sample preparation, the sand was oven-dried at 105 °C for 24 hours. Subsequently, water was added to achieve a sand matrix with a moisture content of 14% (Figure 5a). All prepared roots were cut to 2 cm lengths and sorted by diameter (Figure 5b). During sample preparation, the required soil mass was calculated based on the target dry density. A portion of the soil mass was placed at the bottom of the shear box and compacted with a tamper. Then, prepared roots were embedded in the sand matrix according to the designated scheme. Subsequent soil layers were added and compacted accordingly until the target dry density was achieved (Figure 5d). Direct shear tests were conducted at a shear rate of 0.8 mm/min under normal stresses of 50, 100, and 150 kPa. Shear stress was calculated using Equation (2):

$$\tau = \frac{C \cdot R}{A_0} \times 10 \tag{2}$$

Where τ is the shear stress (kPa), C is the calibration coefficient of the load cell (N/0.01 mm), R is the load cell reading (0.01 mm), and A_0 is the cross-sectional area of the sample (cm²).

Figure 5. Flowchart of the direct shear test.

2.2.3. Test design

In this study, a non-complete block partial-factor experimental design was used to investigate the influence of factors (root diameter, quantity, and orientation) on the shear strength and parameters. According to the principle of space-filling design, 16 representative factor combinations were selected, with each factor combination corresponding to only one sample, and no intra-group repetitions were set up to maximize the breadth of factor level coverage under the limited sample conditions. In the direct shear test, for each sample, 50, 100, and 150 kPa normal stresses were applied to obtain the mechanical responses under different stress states. To quantify the random errors in the sample preparation and testing processes, three independent parallel samples (belonging to the aforementioned 16 factor combinations) were set up for each normal stress level. It should be noted that the "repeatability" of this experiment is reflected in the sample redundancy in the normal stress dimension, rather than the observation replication in the factor combination dimension. The variables investigated in this direct shear test included root diameter (0.5, 1.0, 1.5 mm), root quantity (2, 4, 6), and root distribution orientation (vertical, horizontal, inclined, vertical-horizontal). An L_{16} (4^3) orthogonal test design was adopted. This design allows exploration of the influence of each factor without compromising the study results (Ren *et al.* 2021). As the number of levels differed between factors (4 orientations *vs*. 3 levels for diameter/quantity), the pseudo-level method was applied. The test scheme design and symbol definitions are as follows (Table 2).

Table 2. Experimental design scheme.

Group No.	Root diameter/mm	Root quantity	Root orientation
1	0.5	2	Vertical
2	0.5	4	Horizontal
3	0.5	6	Inclined
4	0.5	6	Vertical-horizontal (cross)
5	1	2	Horizontal
6	1	4	Vertical
7	1	6	Vertical- horizontal (cross)
8	1	6	Inclined
9	1.5	2	Inclined
10	1.5	4	Vertical-horizontal (cross)
11	1.5	6	Vertical
12	1.5	6	Horizontal
13	1	2	Vertical-horizontal (cross)
14	1	4	Inclined
15	1	6	Horizontal
16	1	6	Vertical

3. Results

3.1. Tensile mechanical properties of reinforced sand

The force-displacement curves from the tensile tests are shown in Figure 6. The curves exhibit two distinct stages: an initial tension-increasing stage, during which the tensile force increases continuously with time as the instrument stretches the root, followed by a failure stage, in which the tensile force drops rapidly to zero upon root fracture (Figure 6).

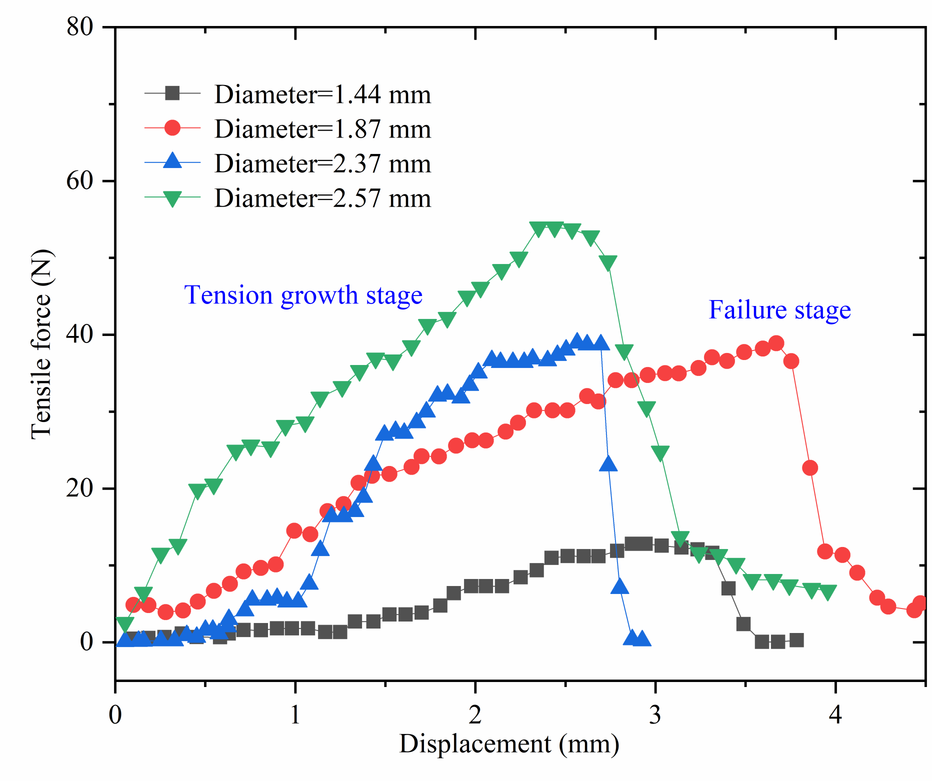

Figure 6. Typical tensile force-displacement curve.

The relationship between maximum tensile force (tensile strength) and root diameter is plotted in Figure 7. It reveals that the maximum tensile force (*F*) of alfalfa roots was linearly and positively correlated with root diameter (d), indicating that *F* increases with increasing *d* (R^2 = 0.8, indicating a good fit). In contrast, root tensile strength (*RM)* exhibited a power function decrease with increasing root diameter, although the relationship was weak (R^2 = 0.24), indicating only a general declining trend.

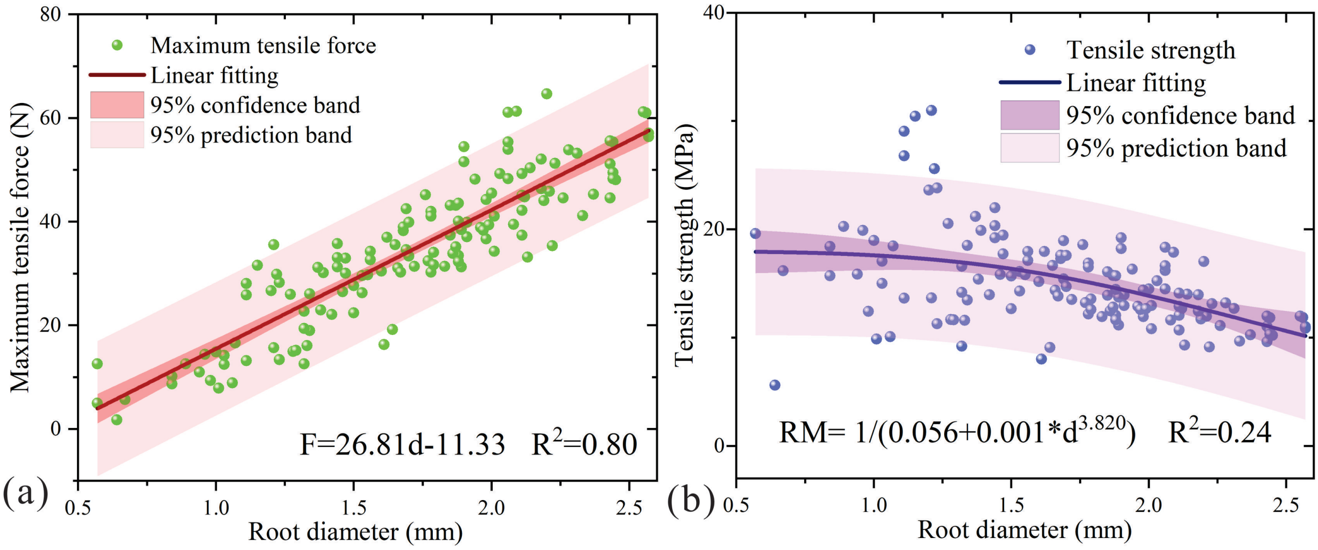

Figure 7. Tensile test results: **(a)** Relationship between maximum tensile force (*F*) and root diameter (*d*); **(b)** Relationship between tensile strength (*RM*) and root diameter (*d*).

3.2. Shear mechanical behavior of root-reinforced sand

Stress–displacement curves were obtained from direct shear tests on the specimens. According to the Geotechnical Test Method Standard (GB/T 50123) (China National Standards 2019), the shear strength was defined as the peak shear stress from the curve; otherwise, the stress corresponding to 4 mm displacement was taken as the shear strength. In the present tests, all stress–displacement curves of the reinforced sand specimens exhibited strain-hardening behavior, with consistent trends across different normal stress levels. Therefore, the results obtained from Group 1 were selected as a representative case for further analysis, as shown in Figure 8. A clear disparity in shear mechanical behavior was observed between unreinforced sand specimens and those reinforced with roots. Under normal stresses of 50, 100, and 150 kPa, the unreinforced soil exhibited a typical strain-softening response, with shear stress rising rapidly to a distinct peak before gradually decreasing, indicating brittle shear failure. The peak shear stress was defined as the shear strength, in accordance with the testing standard, yielding values of 26.9, 53.5, and 80.3 kPa, respectively. Conversely, the root-reinforced specimens exhibited ductile hardening behavior, characterized by a gradual, continuous increase in shear stress with displacement and no obvious peak. For these specimens, the shear strength was therefore taken as the stress at a shear displacement of 4 mm, resulting in corresponding strengths of 38.0, 62.7, and 88.3 kPa.

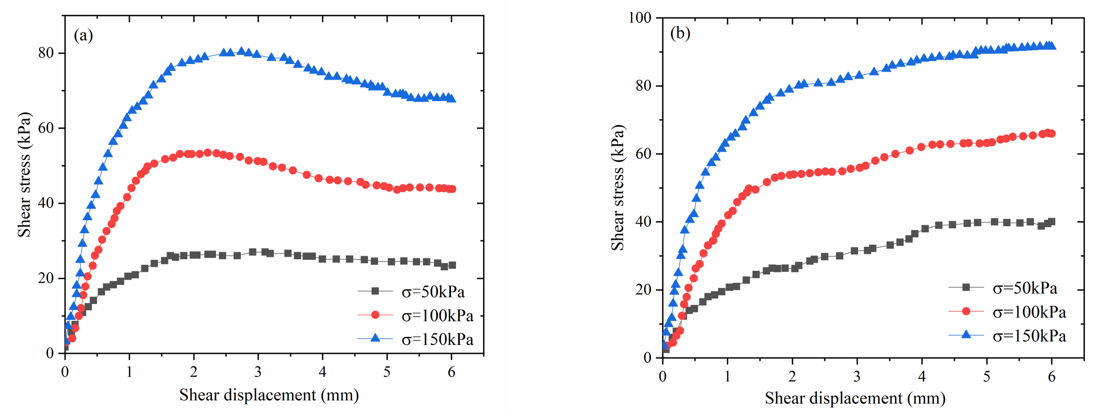

Figure 8. Stress-displacement relationship of specimen **(a)** sand specimen, **(b)** root-reinforced sand specimen.

Furthermore, the shear strength of all specimens under different normal stress levels is shown in Figure 9. Since all reinforced specimens exhibited similar strain-hardening behavior with no distinct peak under normal stresses of 50, 100, and 150 kPa, and the shear strength increased systematically with normal stress (Figure 9), the shear strength parameters of the soil specimen subjected to a normal stress of 150 kPa were selected for subsequent analysis. To analyze shear strength parameter test results more directly and objectively, range analysis was employed to assess the influence of the various factors and to determine the optimal combination. The shear strength (τ), cohesion (c) , and internal friction angle (φ) obtained from each test are detailed in Table 3.

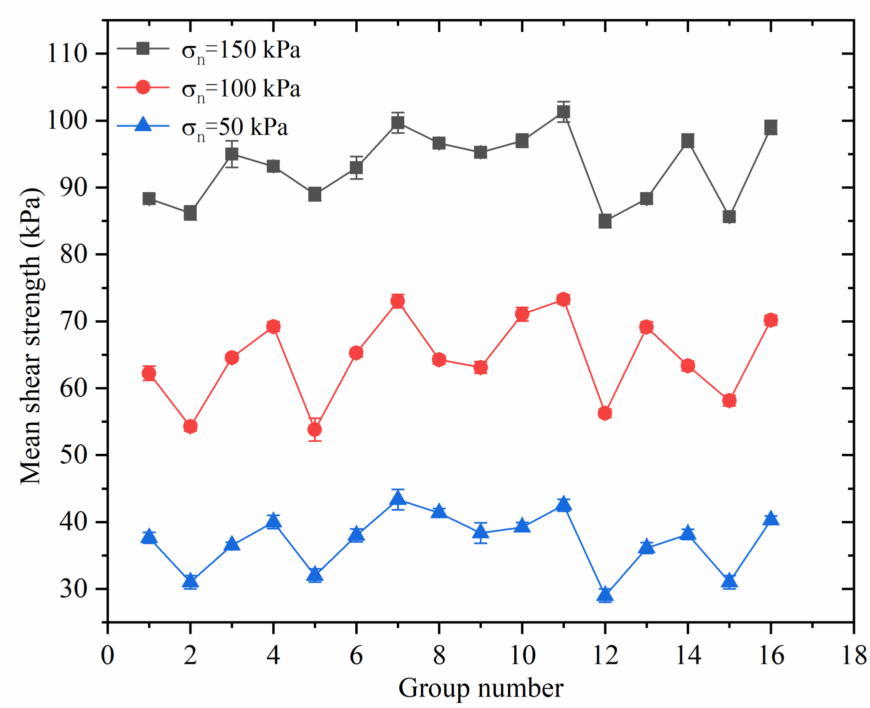

Figure 9. Shear strength of specimens under different normal stresses.

Table 3. Shear strength and strength parameters from the direct shear test.

Group No.	τ	c	ϕ	Group No.	τ	c	ϕ
0	80.3	0	28.19	9	95.3	8.64	32.61
1	88.3	12.04	29.03	10	97.0	11.35	33.09
2	86.2	1.95	31.63	11	101.3	13.57	33.69
3	95.0	6.86	33.52	12	85.0	0.76	32.08
4	93.2	14.29	30.46	13	88.3	12.36	29.89
5	89.0	1.27	32.66	14	97.0	7.34	33.71
6	92.9	10.50	31.47	15	85.6	3.64	31.29
7	99.7	15.67	32.28	16	99.0	11.12	33.63
8	96.6	12.16	31.65				

3.2.1. Range analysis

Range analysis is an important method for analyzing orthogonal test results (Zhou *et al.* 2021). By comparing the range value (R) of the average effects for each factor at different levels, the relative influence of each factor on the results can be assessed. A larger R value indicates a greater influence of that factor on the strength parameter, signifying it as a major factor (Xue *et al.* 2023). As shown in Figure 10, for cohesion, root distribution orientation exerts an overwhelmingly dominant control (R = 11.51), followed by root quantity (R = 1.97) and root diameter (R = 0.68). For the internal friction angle, root diameter acts as the most influential factor (R = 1.71), followed by orientation (R = 1.44) and quantity (R = 1.42). The ranges (R) for all three factors are relatively narrow (spanning from 1.42° to 1.71°), indicating that root parameters have a minor impact on the internal friction angle. For overall shear strength, the global hierarchy of significance follows the sequence of orientation (9.51) > quantity (4.20) > diameter (3.98), demonstrating that the spatial arrangement and orientation of the roots play the most dominant role in enhancing the overall shear strength of the root-soil composite. This finding aligns with classical root-soil mechanics, confirming that roots primarily improve the shear capacity of soil by enhancing cohesion rather than altering the internal friction angle (Schmidt *et al.* 2001; Kokutse *et al.* 2016; Feng *et al.* 2020).

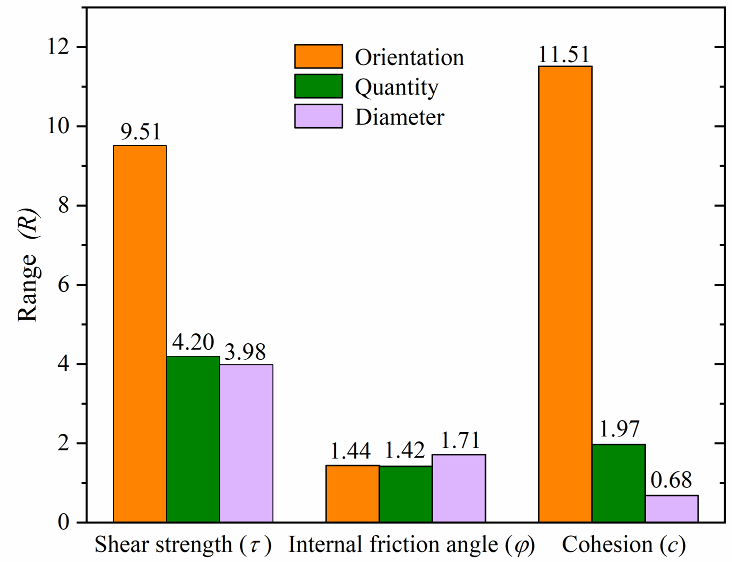

Figure 10. Range analysis of factors affecting shear strength and parameters.

As seen from the orthogonal design (Table 2), for a given level of one factor, the levels of the other two factors are not repeated. For example, when the root diameter is 1 mm, the combinations of root quantity and distribution orientation are unique. Therefore, the mean value of all test results for a factor at a specific level can be considered representative of that factor acting alone at that level (Zhou *et al.* 2021; Xue *et al.* 2023). To more intuitively illustrate the effects of the improvements, the relationships between each factor's level and the shear strength parameters were plotted in Figure 11.

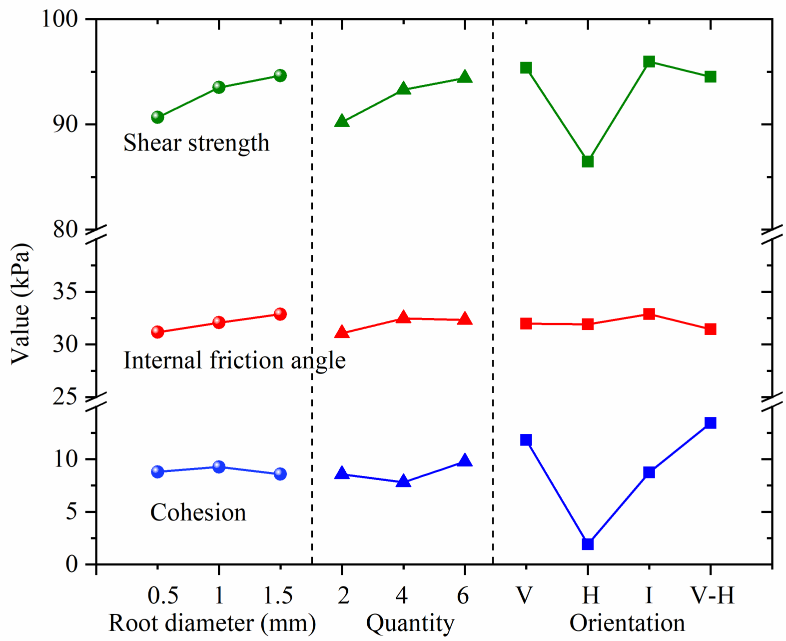

Figure 11. Relationship curves between influencing factors and shear strength, internal friction angle, and cohesion. Note: V-Vertical; H-Horizontal; I-Inclined; V-H-Cross (Vertical-Horizontal).

Based on the control group (Group 0) data in Table 3, the incorporation of the Alfalfa root system led to an overall increase in the shear strength, internal friction angle (φ), and cohesion (c) of the composite soil compared to the unreinforced plain sand. The baseline cohesion of the unreinforced sand was confirmed to be 0 kPa by the control test. Upon root addition, a substantial enhancement in cohesion was observed across most experimental configurations, with all values remaining strictly greater than 0 kPa, except for specific groups with horizontal root distributions, where cohesion dropped to near-zero levels (e.g., 0.76 kPa in Group 12 shown in Table 3).

At a root diameter of 0.5 mm, the shear strength of the root-reinforced specimen increased by 12.92% compared to the plain soil (from 80.3 to 90.67 kPa). At root diameters of 1 mm and 1.5 mm, shear strength further increased by 16.45% and 17.87%, respectively. Variations in root diameter had a minor effect on cohesion and internal friction angle, although both remained higher than those of the plain soil (Figure 11). When the root quantity reached 6, the shear strength of the specimen reached its maximum (94.42 kPa), representing 117.59% of the plain soil. Concurrently, cohesion also reached its maximum (9.76 kPa) among the root quantities. Range analysis indicates that root orientation exerted the most important influence on both shear strength and cohesion. Specifically, when roots were distributed inclined, shear strength reached its maximum (95.96 kPa) among all orientations, corresponding to 119.51% of the plain soil value. However, the horizontal distribution resulted in the minimum shear strength (86.46 kPa) among all rooted groups, though still higher than that of the plain soil. For cohesion, the peak value (13.42 kPa) was attained under the vertical-horizontal (cross) distribution, while the minimum value (1.91 kPa) was obtained under the horizontal distribution (Figure 11). These findings indicate that inclined and vertical arrangements are markedly more effective than the purely horizontal layout in enhancing soil shear strength.

3.2.2. Optimal schemes for enhancing shear strength

The orthogonal direct shear tests demonstrated that root orientation was the most critical factor governing the shear strength and cohesion of the root-soil composite, whereas root diameter exerted a relatively important influence on the internal friction angle. Range analysis revealed that the theoretical optimal combination for maximizing the overall shear strength was identified as a 1.5 mm root diameter, 6 roots, and an inclined orientation (Figure 11).

4. Discussion

4.1. Mobilization of tensile stress and anchoring mechanism

The role of roots within root-soil composites can be analogous to "reinforcement" in reinforced soil. According to the tensile test results (Figure 6), roots possess a substantial capacity to withstand tensile forces. When root-reinforced soil is subjected to shear deformation, roots experience lateral pressure and/or friction from soil particles, causing them to deform along the shear direction, which progressively mobilizes tensile stresses within the root fibers before any structural rupture occurs (Fan and Tsai 2016). The generated tensile force acts as a counteractive vector against the external shear stress, fundamentally increasing the macroscopic shear behavior of the composite (Masi *et al.* 2021). Thus, roots function via a tensioning and anchoring framework. Once roots were sufficiently anchored within the sand, the axial root tension provided an effective confining pressure that inhibited shear failure. This mechanism resembles embedding numerous tensile "anchor rods" within the sand, binding no cohesive particles into a stable, unified structure (Wang *et al.* 2021).

Consistent with previous findings, the tensile test results showed that larger root diameters contribute to greater maximum tensile force (Bischetti *et al.* 2005; Mao *et al.* 2018). However, tensile strength (*RM*) tends to decrease with increasing diameter. This negative correlation may be a biological trade-off, where thicker roots often undergo enhanced lignification, leading to enlarged hollow medullary zones and decreased cellulose density per unit area, whereas finer roots possess denser cell wall architectures and higher specific strength (Flores and Friswell 2013; Mao *et al.* 2018). Additionally, the high data dispersion demonstrates that *RM* is affected by non-geometric factors, such as root development stage, aging, and micro-structural heterogeneity (Loades *et al.* 2015).

Range analysis of the orthogonal direct shear tests proved that root orientation was the primary factor governing both composite shear strength and cohesion. When roots are oriented vertically or inclined relative to the shear direction, the progressive shear displacement stretches the fibers, mobilizing their anchoring force (Wang *et al.* 2021). This explains why the theoretical optimal configuration for maximizing shear strength was identified as A3B3C3 (1.5 mm diameter, 6 roots, and inclined orientation), and why the absolute peak shear strength (101.3 kPa) was obtained in the vertical arrangement of Group 11 (1.5 mm, 6 roots). Under these alignments, larger root diameters provide higher absolute tensile anchors (*F*) to resist shearing, despite their lower relative tensile strength (*RM*).

Conversely, horizontally oriented roots interact with the soil primarily via interfacial sliding friction. As shear displacement induces negligible axial stretching in this alignment, the mobilized tensile force remains low, yielding a minimal improvement in shear parameters. When roots are distributed vertically and horizontally (cross), a distinct structural interlocking mechanism emerges. Beyond the axial tension of vertical segments, the orthogonal roots mutually constrain each other under shear deformation. This spatial confinement forces the horizontal segments to stretch and develop secondary tensile resistance through spatial interlocking (Figure 12a). Beyond anchorage between roots and soil, an additional binding force is generated to resist shear. This binding mechanism explains why the vertical-horizontal network (Group 7: 1.0 mm, 6 roots) yielded the maximum apparent cohesion (15.67 kPa) among all testing groups.

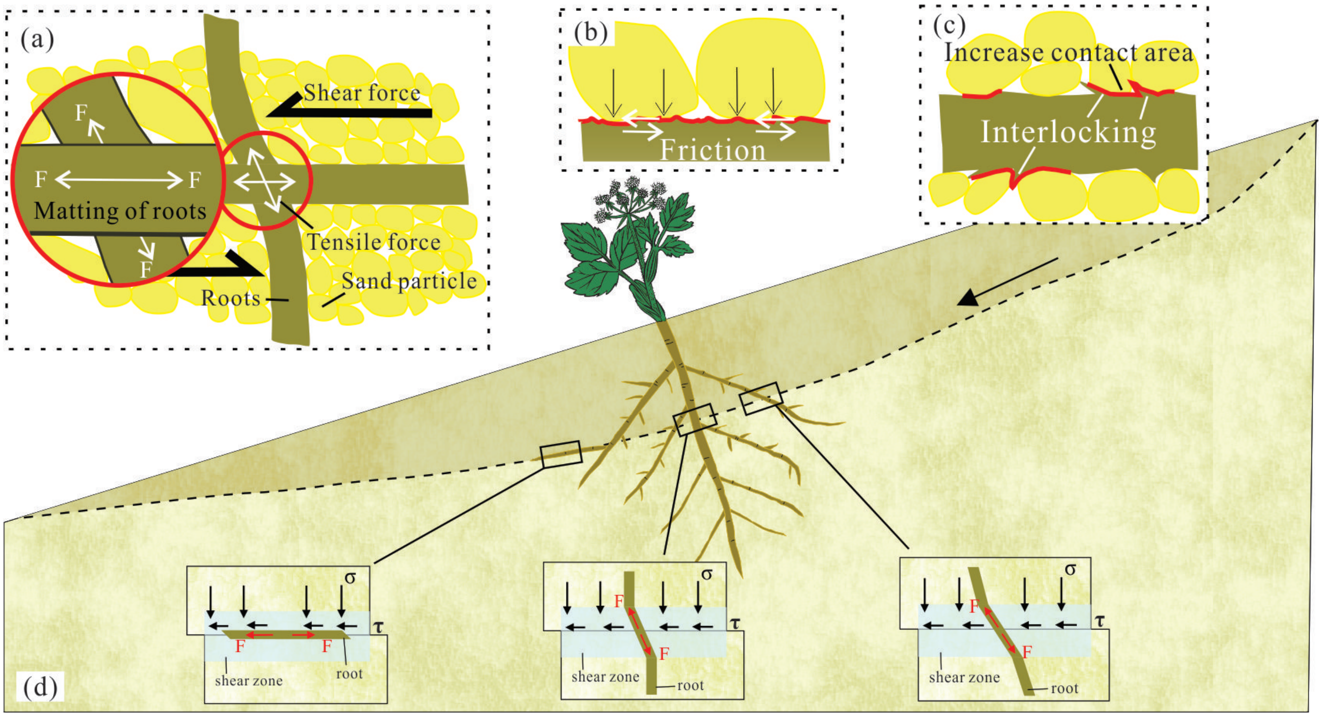

Figure 12. Schematic diagram of root-soil reinforcement mechanisms.

4.2. Root-soil friction

Internal shear friction between the embedded roots and surrounding sand particles plays an important role in stress transfer (Figure 12b). Under an applied horizontal shear force, the relative displacement of sand particles is physically impeded by the root-soil interfacial friction, which effectively mobilizes the tensile capacity of the root fibers to counteract the external shearing force (Caine 1989). As demonstrated by the range analysis, this interfacial frictional resistance does not fundamentally alter the internal friction angle of the root-reinforced specimens, which remains relatively stable. Instead, the geometric-mechanical coupling effect of larger root diameters and higher root quantities acts to suppress soil dilatancy and restrict particle slippage along the shear plane. This structural constraint was manifested macroscopically primarily as an enhancement in the apparent cohesion, rather than a change in the internal friction angle (Figure 10). This behavior is consistent with the single-root tensile results, where thicker roots provided a substantially higher ultimate tensile force (Figure 7a), thereby exerting a stronger reinforcing effect. Consequently, increasing both the root quantity and diameter expands the total interfacial shearing zone (Cazzuffi *et al.* 2014), enhancing the apparent cohesion of the root-reinforced sand matrix, and ultimately improving the overall shear strength.

The stable internal friction angle and enhanced cohesion observed in this study align with findings from alternative coarse-grained matrices, such as silty sand, where root inclusions inflate the failure envelope exclusively via cohesive development without altering mineral sliding friction (Ali and Osman 2008). Furthermore, the observed sensitivity to root orientation is strongly corroborated by fine-grained literature. Crucially, this reinforcement efficiency remains highly sensitive to spatial architecture rather than generalized volume. Triaxial testing on reinforced loess confirms that vertical and crossed architectures maximize shear resistance (Lian *et al.* 2019). In contrast, horizontal arrangements—particularly in cohesive clay soil—can introduce weak, smooth sliding planes that lower shear impedance (Ghestem *et al.* 2014).

4.3. Structural Interlocking

The morpho-structural geometric variations and macroscopic surface texture of roots enable them to establish a structural interlocking network within the sand matrix. At the grain-scale interface, microscopic surface asperities, branch junctions, and localized cortical protrusions increase the root–soil interfacial friction coefficient and provide additional mechanical interlocking points, thereby enhancing the efficiency of shear stress transfer across the root–soil interface. During shear deformation, these interlocked root-soil boundaries function analogously to a rigid mechanical assembly. This boundary coupling stabilizes the mineral skeletal framework of the soil, actively restricts progressive particle rotation and sliding displacement, and provides exceptional resistance against lateral shear strain propagation (Figure 12c).

Range analysis results indicate that vertically and inclinedly distributed roots contribute most significantly to the enhancement of shear strength, whereas the vertical–horizontal (V-H) distribution exhibits the most pronounced improvement in cohesion (Figure 10). This directional dependency further corroborates the key role of root spatial configuration in dictating reinforcement efficiency. Specifically, under the V-H cross distribution, orthogonally arranged root segments intertwine to form a coherent three-dimensional spatial network, which acts as a structural cage that substantially enlarges the spatial confinement imposed on the cohesionless sand particles. Crucially, consistent with numerous classical soil-bioengineering studies (Lal 1998; Wang *et al.* 2019), the experimental results generated from this investigation indicate that this geometric interlocking does not alter the fundamental mineral-to-mineral sliding friction or the basic contact properties of the sand grains. Consequently, the internal friction angle remains relatively unchanged across all network densities. In contrast, the macroscopic structural constraint induced by this interfacial interlocking is manifested almost exclusively as a pronounced increase in the apparent cohesion of the composite material. This orientation-dependent characteristic is quantified by our direct shear test results: Group 12 (1.5 mm, 6 roots, Horizontal) exhibited a negligible cohesion of only 0.76 kPa, despite possessing the maximum total root mass, where the horizontal interfaces instead acted as a weak sliding plane. In contrast, Group 1 (0.5 mm, 2 roots), which had a much lower total root density but a vertical alignment, achieved a remarkably higher cohesion of 12.04 kPa due to the direct mobilization of the doweling effect across the shear plane.

It is worth noting that while root diameter and root quantity were investigated as independent factors in this orthogonal experiment (Table 2), the joint metric of root area ratio (*RAR*) or root density is widely recognized as a fundamental parameter in classical root-soil mechanical models (Leung *et al.* 2017). In this study, decoupling diameter and quantity further reveals structural insights that a single lumped *RAR* or root density masks. For instance, comparing the inclined groups-Group 3 (0.5 mm, 6 roots) and Group 9 (1.5 mm, 2 roots), which obliquely intersect the shear plane, Group 9's total root area is roughly three times that of Group 3. However, their cohesion (c = 6.86 *vs.* 8.64 kPa) did not scale proportionally. This indicates that while thicker roots (Group 9) offer higher bending stiffness and shear-slip resistance, a higher quantity of finer roots (Group 3) optimizes the reinforcement by significantly expanding the root-soil interface friction and contact area per unit volume. Consequently, conventional root-soil mechanical models (e.g., the Wu-Waldron Model) (Mao 2022), which rely on a generalized, isotropic *RAR* to govern mobilized tensile resistance, may not fully account for the anisotropic behavior of these composites. Interfacial sliding friction, axial tensioning, and structural interlocking tend to be more effectively mobilized when the root phase forms a significant angle with the shear trajectory, whereas their contribution may be relatively limited when the roots are oriented parallel to the shear direction.

In summary, the spatial orientation of roots relative to the shearing plane dictates the cooperative efficiency and mobilization sequence of the reinforcement mechanisms. The root-soil interfacial sliding friction, axial tensioning, and structural interlocking can be fully mobilized only when the root phase forms a significant angle with the shear direction (e.g., vertical and inclined configurations), thereby enhancing the shear strength. Meanwhile, the three-dimensional interlocking grid of cross (V-H) networks selectively optimizes the apparent cohesion. In contrast, when roots are aligned parallel to the shear direction (horizontal), the axial tensioning and anchoring effects become entirely negligible, resulting in the weakest enhancement in overall shear strength (Figure 12). Therefore, future predictive frameworks must transcend generalized *RAR* by integrating three-dimensional spatial orientation with localized, effective cross-plane density metrics to accurately reflect eco-geotechnical reinforcement efficiency.

4.4. Limitations of the study

In this study, the root distribution patterns on the shear strength of the root-reinforced sand were investigated. Direct shear tests were performed using manually cut, uniform root segments with a 2 cm length, which were placed along four directional layouts: vertical, horizontal, inclined, and vertical-horizontal. Nevertheless, natural *in-situ* root systems are characterized by complex branching architectures, winding root curvatures, variable diameters, and spatial heterogeneity (Fitter 2002; Hinsinger *et al.* 2005). Such simplifications of root orientation in laboratory direct shear tests aim to isolate and quantify the specific mechanics of root reinforcement. By controlling root length, diameter, and orientation as independent variables, the present study successfully isolates the geometric mechanisms of stress mobilization without the confounding effects of natural geometric variability. While these laboratory findings provide fundamental mechanical insights into orientation-dependent reinforcement, future studies are needed to focus on capturing the mechanical responses generated by complex, spatially heterogeneous natural root networks. Furthermore, long-term field lysimeters and macro-scale monitoring are highly needed to bridge the gap between laboratory-scale mechanisms and field-scale ecological engineering applications.

5. Conclusion

This study investigated the tensile mechanical properties and shear behavior of root-reinforced sandy soil through a series of root tensile tests and orthogonal direct shear tests. The main conclusions are as follows:

(1) The root tensile tests demonstrated that, within the tested diameter range, the maximum peak tensile force (*F*) exhibits a positive linear correlation with root diameter (*d*), adhering to the empirical relation $F = 26.81d - 11.33$. Conversely, the ultimate tensile strength (*RM*) decays nonlinearly with increasing diameter.

(2) Range analysis of the orthogonal direct test results revealed that root spatial orientation was identified as the governing factor controlling both composite shear strength and apparent cohesion, with the order of influence being Orientation > Quantity > Diameter. Critically, root inclusions primarily augment the ultimate shear strength by enhancing the apparent cohesion, with negligible variation in the internal friction angle. Although Group 11 with vertically arranged roots recorded the highest experimental shear strength of 101.3 kPa, theoretical calculation reveals that the optimal configuration for maximizing overall shear strength is identified as a root diameter of 1.5 mm, a quantity of 6, and an inclined orientation. In contrast, a three-dimensional vertical-horizontal (cross) network selectively optimizes cohesion, yielding a peak cohesion of 15.67 kPa in Group 7.

(3) The composite shear strength enhancement is governed by a cooperative macroscopic mechanism involving interface friction, axial tensioning/anchoring, and structural interlocking. Root-reinforced sand behaves as an anisotropic, parameter-specific system rather than a uniform strength upgrade. Specifically, the axial tensioning and anchoring efficiency are optimized when the root fibers form a significant angle relative to the shearing plane (vertical or inclined), under which alignment thicker roots supply superior absolute tensile capacity (*F*) to resist shearing vectors despite their lower relative material strength (*RM*). Conversely, three-dimensional orthogonal grids selectively maximize apparent cohesion via spatial cross-linking. These findings imply that accurate constitutive modeling of root-reinforced sand should incorporate spatial network geometry. Beyond theoretical insights, this parameter-specific divergence provides a practical method for desert subgrade stabilization. Replacing high-density vegetation planting with geometry-optimized root deployment offers an economic and ecologically sustainable strategy to maximize slope reinforcement under hyper-arid, resource-constrained engineering conditions.

Data availability statement

The data or datasets that support the findings of this study are available from the corresponding author upon reasonable request.

Declaration of generative AI and AI-assisted technologies

During the preparation of this manuscript, the authors used Grammarly only to improve language and readability in limited sections of the manuscript. Generative AI was not used for data generation, data analysis, interpretation of results, or the development of scientific conclusions. The authors take full responsibility for the content of the manuscript.

Acknowledgments

Financial support of National Key R&D Program of China (Grant No. 2023YFC3008400) is gratefully acknowledged.

Authors' contribution

Baoqin Lian: conceptualization, formal analysis, software, writing—original draft, writing—review and editing; Chaoying Gu: methodology, data curation, writing—original draft; Xingang Wang: conceptualization, methodology, supervision, funding acquisition; Haoyu Wang; methodology, investigation. All authors have read and agreed to the published version of the manuscript.

Conflicts of interest

The authors declare no conflicts of interest.

References

Ali FH, Osman N. Shear strength of a soil containing vegetation roots. *Soils Found.* 2008, 48(4):587–596. DOI: 10.3208/sandf.48.587

Bischetti GB, Chiaradia EA, Simonato T, Speziali B, Vitali B, *et al*. Root strength and root area ratio of forest species in Lombardy (Northern Italy). *Plant Soil* 2005, 278(1):11–22. DOI: 10.1007/s11104-005-0605-4

Caine N. Slope stability: geotechnical engineering and geomorphology. *Quat. Sci. Rev.* 1989, 8(1):104–105. DOI: 10.1016/0277-3791(89)90029-2

Cazzuffi D, Cardile G, Gioffrè D. Geosynthetic engineering and vegetation growth in soil reinforcement applications. *Transp. Infrastruct. Geotechnol.* 2014, 1(3):262–300. DOI: 10.1007/s40515-014-0016-1

China National Standards. Standard for geotechnical testing method (GB/T 50123-2019). 2019. Available: https://www.gbstandards.org/GB_standard_english.asp?code=GB/T%2050123-2019 (accessed on 8 July 2026).

Duan X, Yang Z, Wang B, Chen C, Qu J, *et al.* Time-varying tensile resistance mechanisms in slope-protecting alfalfa roots. *Plant Soil* 2026, 521:1937–1957. DOI: 10.1007/s11104-026-08494-8

Fan CC, Su CF. Role of roots in the shear strength of root-reinforced soils with high moisture content. *Ecol. Eng.* 2008, 33(2):157–166. DOI: 10.1016/j.ecoleng.2008.02.013

Fan CC, Tsai MH. Spatial distribution of plant root forces in root-permeated soils subject to shear. *Soil Tillage Res.* 2016, 156:1–15. DOI: 10.1016/j.still.2015.09.016

Feng S, Liu H, Ng CWW. Analytical analysis of the mechanical and hydrological effects of vegetation on shallow slope stability. *Comput. Geotech.* 2020, 118:103335. DOI: 10.1016/j.compgeo.2019.103335

Fitter A. Characteristics and functions of root systems. Characteristics and functions of root systems. *In Plant Roots: The Hidden Half*, 3rd ed. Boca Raton: CRC Press, 2002. pp. 49–78.

Flores EIS, Friswell MI. Ultrastructural mechanisms of deformation and failure in wood under tension. *Int. J. Solids Struct.* 2013, 50(13):2050–2060. DOI: 10.1016/j.ijsolstr.2013.03.003

Gao S, Wang Y, Zhang L, Gong X, Zhang Q. Introduction to sand-restoration technology and model in China. *Sustainability* 2022, 15(1):98. DOI: 10.3390/su15010098

Garg A, Leung AK, Ng CWW. Transpiration reduction and root distribution functions for a non-crop species Schefflera heptaphylla. *Catena* 2015, 135:78–82. DOI: 10.1016/j.catena.2015.06.019

Ghestem M, Veylon G, Bernard A, Vanel B, Stokes A. Influence of plant root system morphology and architectural traits on soil shear resistance. *Plant Soil* 2014, 377(1):43–61. DOI: 10.1007/s11104-012-1572-1

Hinsinger P, Gobran GR, Gregory PJ, Wenzel WW. Rhizosphere geometry and heterogeneity arising from root-mediated physical and chemical processes. *New Phytol.* 2005, 168(2):293–303. DOI: 10.1111/j.1469-8137.2005.01512.x

Kokutse NK, Temgoua AGT, Kavazović Z. Slope stability and vegetation: Conceptual and numerical investigation of mechanical effects. *Ecol. Eng.* 2016, 86:146–153. DOI: 10.1016/j.ecoleng.2015.11.005

Lal R. Biotechnical and Soil bioengineering slope stabilization: a practical guide for erosion control. *Soil Sci.* 1998, 163(1):83–85. DOI: 10.1097/00010694-199801000-00012

Leung AK, Kamchoom V, Ng CWW. Influences of root-induced soil suction and root geometry on slope stability: a centrifuge study. *Can. Geotech. J.* 2017, 54(3):291–303. DOI: 10.1139/cgj-2015-0263

Li R, Kan S, Zhu M, Chen J, Ai X, *et al*. Effect of different vegetation restoration types on fundamental parameters, structural characteristics and the soil quality index of artificial soil. *Soil Tillage Res.* 2018, 184:11–23. DOI: 10.1016/j.still.2018.06.010

Lian B, Peng J, Zhan H, Wang X. Mechanical response of root-reinforced loess with various water contents. *Soil Tillage Res.* 2019, 193:85–94. DOI: 10.1016/j.still.2019.05.025

Liu S, Ni J, Zhang X, Gao Y, He N, *et al*. A new and simple hypoplastic model for saturated soils reinforced by plant roots. *Comput. Geotech.* 2026a, 190:107725. DOI: 10.1016/j.compgeo.2025.107725

Liu S, Ni J, Gao Y, He N, Deng Y. Hypoplastic modelling of thermo-mechanical behavior of root-reinforced soils. *Can. Geotech. J.* 2026b, 63:1–26. DOI: 10.1139/cgj-2025-1092

Loades KW, Bengough AG, Bransby MF, Hallett PD. Effect of root age on the biomechanics of seminal and nodal roots of barley (*Hordeum vulgare L.*) in contrasting soil environments. *Plant Soil* 2015, 395(1):253–261. DOI: 10.1007/s11104-015-2560-z

Mao Z. Root reinforcement models: Classification, criticism and perspectives. *Plant Soil* 2022, 472(1):17–28. DOI: 10.1007/s11104-021-05231-1

Mao Z, Wang Y, McCormack ML, Rowe N, Deng X, *et al*. Mechanical traits of fine roots as a function of topology and anatomy. *Ann. Bot.* 2018, 122(7):1103–1116. DOI: 10.1093/aob/mcy076

Masi EB, Segoni S, Tofani V. Root reinforcement in slope stability models: a review. *Geosciences* 2021, 11(5):212. DOI: 10.3390/geosciences11050212

Ng CWW, Kamchoom V, Leung AK. Centrifuge modelling of the effects of root geometry on transpiration-induced suction and stability of vegetated slopes. *Landslides* 2016, 13(5):925–938. DOI: 10.1007/s10346-015-0645-7

Ni J, Zhang W, Liu S, Deng Y, He N. Experimental and DEM investigation of root orientation effects on shear behavior of soils subjected to freeze–thaw cycles. *Eng. Geol.* 2025, 359:108433. DOI: 10.1016/j.enggeo.2025.108433

Operstein V, Frydman S. The influence of vegetation on soil strength. *Proc. Inst. Civ. Eng. Ground Improv.* 2000, 4(2):81–89. DOI: 10.1680/grim.2000.4.2.81

Pollen N. Temporal and spatial variability in root reinforcement of streambanks: accounting for soil shear strength and moisture. *Catena* 2007, 69(3):197–205. DOI: 10.1016/j.catena.2006.05.004

Qi Y, Chang Q, Jia K, Liu M, Liu J, *et al*. Temporal-spatial variability of desertification in an agro-pastoral transitional zone of northern Shaanxi Province, China. *Catena* 2012, 88(1):37–45. DOI: 10.1016/j.catena.2011.08.003

Ren W, Yang T, Huang M, Zhang A, Wei H, *et al*. Optimal mixing ratio and SWCC fitting of lightweight soil with cotton stalk fibres. *Soils Found.* 2021, 61(2):453–464. DOI: 10.1016/j.sandf.2021.01.004

Sanchez-Castillo L, Kosugi K, Masaoka N, Kubota T. Eco-morphological characteristics of fern species for slope conservation. *J. Mt. Sci.* 2019, 16(3):504–515. DOI: 10.1007/s11629-018-5106-z

Schmidt KM, Roering JJ, Stock JD, Dietrich WE, Montgomery DR, *et al*. The variability of root cohesion as an influence on shallow landslide susceptibility in the Oregon Coast Range. *Can. Geotech. J.* 2001, 38(5):995–1024. DOI: 10.1139/t01-031

Wang F, Zhao M, Sun Q. Experimental study on shear resistance of Carex-Root-Fibered Soil. *Adv. Civ. Eng.* 2021, 2021(1):6680204. DOI: 10.1155/2021/6680204

Wang X, Zhang C, Hasi E, Dong Z. Desertification in China: an assessment. *Earth Sci. Rev.* 2008, 88(3–4):188–206. DOI: 10.1016/j.earscirev.2008.02.001

Wang X, Hong M, Huang Z, Zhao Y, Ou Y, *et al*. Biomechanical properties of plant root systems and their ability to stabilize slopes in geohazard-prone regions. *Soil Tillage Res.* 2019, 189:148–157. DOI: 10.1016/j.still.2019.02.003

Wang X, Ma C, Wang Y, Wang Y, Li T, *et al*. Effect of root architecture on rainfall threshold for slope stability: variabilities in saturated hydraulic conductivity and strength of root-soil composite. *Landslides* 2020, 17(8):1965–1977. DOI: 10.1007/s10346-020-01422-6

Xue C, Wang X, Lian B, Luo L, Liu K. Research on the mechanism of composite improvement of loess based on quantitative analysis of microstructure and mechanical strength. *Constr. Build. Mater.* 2023, 379:131215. DOI: 10.2139/ssrn.4257143

Zhou Z, Li F, Yang H, Gao W, Miao L. Orthogonal experimental study of soil–rock mixtures under the freeze–thaw cycle environment. *Int. J. Pavement Eng.* 2021, 22(11):1376–1388. DOI: 10.1080/10298436.2019.1686634